



City Research Online

## City, University of London Institutional Repository

---

**Citation:** Gabdullin, N & Khan, S. (2016). Study of Non-Homogeneity of Magnetic Field Distribution in Single-Crystal Ni-Mn-Ga Magnetic Shape Memory Element in Actuators due to its Anisotropic Twinned Microstructure. *IEEE Transactions on Magnetics*, 53(3), 4900108. doi: 10.1109/tmag.2016.2640201

This is the accepted version of the paper.

This version of the publication may differ from the final published version.

---

**Permanent repository link:** <https://openaccess.city.ac.uk/id/eprint/16066/>

**Link to published version:** <https://doi.org/10.1109/tmag.2016.2640201>

**Copyright:** City Research Online aims to make research outputs of City, University of London available to a wider audience. Copyright and Moral Rights remain with the author(s) and/or copyright holders. URLs from City Research Online may be freely distributed and linked to.

**Reuse:** Copies of full items can be used for personal research or study, educational, or not-for-profit purposes without prior permission or charge. Provided that the authors, title and full bibliographic details are credited, a hyperlink and/or URL is given for the original metadata page and the content is not changed in any way.

---

City Research Online:

<http://openaccess.city.ac.uk/>

[publications@city.ac.uk](mailto:publications@city.ac.uk)

---

# Study of Non-Homogeneity of Magnetic Field Distribution in Single-Crystal Ni-Mn-Ga Magnetic Shape Memory Element in Actuators due to its Anisotropic Twinned Microstructure

N. Gabdullin, *Student Member, IEEE*, S. H. Khan, *Member, IEEE*

School of Mathematics, Computer Science and Engineering, City, University of London, London EC1V 0HB, UK

Magnetic shape memory (MSM) alloys are relatively new and very promising “smart” materials which respond to magnetic fields and exhibit the shape memory effect at room temperature. Maximum strain varies from 6 to 12% of the MSM element’s length depending on its microstructure. The shape memory effect and magnetic field-induced reorientation of MSM twin variants in low-temperature martensite phase are subject to an ongoing research for almost two decades. However, the magnetic field distribution in the MSM elements and effects of its varying magnetic permeability on bias magnetic field are not well studied. In this paper we present an extension to the existing modeling approach for MSM elements applicable to actuator design. The effects arising from single-crystal anisotropy and demagnetization effects due to non-homogeneous multi-variant MSM microstructure are studied and discussed. The proposed approach is validated by comparing computational results with previously reported measurement data.

**Index Terms**—Magnetic shape memory (MSM) alloys, MSM actuators, electromagnetic analysis, non-homogeneous permeability, magnetic anisotropy

## I. INTRODUCTION

MAGNETIC shape memory (MSM) “smart” alloys form a new class of shape memory materials which respond to magnetic fields. MSM alloys can also be controlled mechanically, and both magnetically and mechanically induced stresses are coupled [1]. Ni-Mn-Ga alloys are the most studied MSM alloys which exhibit enormous 6-12% maximum magnetic field induced strain (change in shape) depending on specimen microstructure [2], [3]. Whereas MSM effect is very sensitive to temperature [4], MSM alloys are potentially capable of very long fatigue life which makes them very promising for use in actuators and sensors in a frequency range up to several kHz [5]. MSM actuators are high-performance, fast and compact, energy efficient and reliable. However, there is still lack of a consistent methodology for designing MSM actuators limiting the development in the area of MSM application. This is partially due to lack of a well-established modeling approach for the MSM element and its interaction with the rest of actuator’s magnetic circuit.

MSM elements used in actuators are commonly produced as single crystals which have tetragonal lattice in low-temperature martensite phase. The shape change in magnetic fields occurs due to inequality in lattice parameters coupled with magnetic anisotropy of the crystal [6]. A short

crystallographic  $c$  axis, which is also “easy” magnetization axis, tends to align with the applied magnetic field. This may result in local reorientation of the crystal [7]. Since “hard” magnetization  $a$  and  $b$  axes are longer than  $c$  axis, local reorientation of the crystal results in overall elongation or contraction. It should be noted that only the most studied 5-layered modulated (5M) Ni-Mn-Ga microstructure with lattice parameters  $a=b$  and  $c/a=0.94$  is considered in this study. The maximum change in shape (strain) is related to the ratio of crystallographic parameters as  $\varepsilon_{max}=1-c/a$  which implies 6% maximum output strain for 5M crystals. However, MSM microstructure is formed of multiple areas with different orientation of crystallographic  $c$  axes called twin variants in any intermediate state when not fully contracted or elongated (see Fig. 1). Variants which have their “easy” axes aligned with the applied magnetic field are commonly referred to as “easy” variants, whereas “easy” axes are transverse to the bias field in “hard” variants. As intensity of the applied magnetic field increases, “easy” variants grow at expense of “hard” variants until a single variant of one type is present [2]. The magnetic field is usually applied transverse to the longest side of a tetragonal MSM element for producing output strain in MSM actuators (see Fig 1. (a)). Output strain and stress production is possible as long as “hard” variants exist. However, a magnetic field applied along the MSM element results in its contraction, as shown in Fig. 1 (b). This phenomenon is a direct consequence of the magnetic anisotropy of MSM twin variants, since variants favored by transversely applied magnetic field are not favorable for longitudinal fields. It should be noted that only the abovementioned macroscopic “hard” and “easy” twin variants are considered in this study.

**Fig. 1 HERE**

## II. MODELLING THE MSM ELEMENT IN ACTUATORS

### A. Magnetic Field Formulation

Finite element (FE) analysis is applied for solving magnetostatic problem associated with the magnetic field distribution in the MSM element. A small 2.5 mm × 1 mm MSM element is used for clarity of the pictures in all 2D FE models (see Fig. 2). The magnetic field is applied transversely to the MSM element in all experiments.

A set of magnetic field equations to be solved comprises two Maxwell's equations and one constitutive relationship:

$$\nabla \times \mathbf{H} = \mathbf{J} \quad (1)$$

$$\nabla \cdot \mathbf{B} = 0 \quad (2)$$

$$\mathbf{B} = \mu \mathbf{H} \quad (3)$$

where  $\mathbf{H}$  is magnetic field intensity, A/m,  $\mathbf{J}$  is current density, A/m<sup>2</sup>,  $\mathbf{B}$  is magnetic flux density, T. A magnetic vector potential (MVP) formulation is used for solving the above equations

$$\mathbf{B} = \nabla \times \mathbf{A} \quad (4)$$

where  $\mathbf{A}$  is magnetic vector potential, Wb/m. Equation (1) combined with (3) and (4) yields a vector Poisson's equation

$$\nabla^2 \mathbf{A} = -\mu \mathbf{J} \quad (5)$$

Dirichlet boundary conditions are applied on outer boundaries in the models. Equation (5) is solved using the FEM modeling capabilities of ANSYS Multiphysics software package. Solutions for  $\mathbf{B}$  and  $\mathbf{H}$  fields are derived based on the solution obtained for the magnetic vector potential.

### B. MSM Microstructure and Properties

Many studies on the behavior of the MSM element in a bias magnetic field can be found e.g., [1], [8], [9]. However, only a few papers analyzing the MSM element as part of an actuator or sensor have been published so far. When analyzed as part of a complete magnetic circuit, properties of the MSM element affect the total reluctance and, hence the total magnetic field produced by coils and/or permanent magnets. Demagnetization effects related to MSM element's shape also make the understanding of magnetic field distribution in the MSM region based on measurement results challenging [10]. There is a considerable difference between the magnetic field in the MSM element and the magnetic field that can be measured in the air gap. The significance of demagnetization and challenges associated with capturing related effects in analytical models have been mentioned numerous in publications e.g., [10]–[12]. However, effects related to

geometry, non-homogeneity, anisotropy and non-linearity of magnetic characteristics can easily be taken into account in a FE model, a solution for which is obtained using numerical methods. A complete magnetic circuit including the MSM element can be incorporated in a single model, which is vital for actuator design (see Fig. 2). Such an approach was recently developed by Schiepp *et al.* [13]. However, the anisotropy of MSM twin variants and, hence its effects on magnetic field distribution is not captured in the existing modeling approaches.

It is necessary to incorporate the geometry and magnetic anisotropy of twin variants in order to accurately model the transverse magnetic field distribution inside a non-homogeneous MSM element. We model the twin variant distribution through breaking the MSM element into thin bands corresponding to different twin variants [13] using the known geometry of each variant [14]. Each variant is treated as anisotropic and magnetic properties are assigned according to the current orientation of crystallographic axes inside a variant. Magnetization B-H curves in Fig. 2 were used for “easy” and “hard” magnetization axes. The initial slopes of the “hard” and “easy” curves correspond to relative permeability  $\mu_h=2$  and  $\mu_e=50$ , whereas saturation magnetization  $M_s=0.69$  T. This allows representing a non-homogeneous MSM region as a mixture of homogeneous yet anisotropic twin variants.

**Fig. 2 HERE**

It should be stressed that both “easy” and “hard” axes' B-H curves are used for each variant as shown in Fig. 2, since even a single-variant MSM element still exhibits anisotropy. This also allows taking into account non-linearity of their magnetic properties which is particularly important for highly susceptible “easy” axis. However, the behavior of “hard” axis permeability is linear in magnetic fields below 550 kA/m. This allows linearization of its B-H curve in weaker fields. Fig. 2 shows that magnetic field lines tend to align with the initial orientation of the bias field in a single-variant MSM element. The disturbance due to the presence of “easy” axis inside a “hard” variant is minor since only one variant exists. However, Fig. 3 and 4 illustrate the considerable differences in magnetic field distribution inside and outside the MSM element when it is in a multi-variant state.

**Fig. 3 HERE****Fig. 4 HERE**

The distribution of MSM twin variants is modeled only approximately in this approach. However, the magnetic field

distribution in the MSM element with many twin bands is very different from one associated with a single twin boundary, as shown in Figs. 3 and 4. Twin variants in MSM elements with stable Type I twin boundaries tend to form lamellar structures [15]. Therefore, the results obtained through modeling fine twins in Fig. 3 are applicable to actuator design. Nevertheless, the same approach can be used for analyzing the behavior of MSM elements with a single Type II twin boundary in Fig. 4. A position of the boundary can be adjusted for studying the related effects on switching field discussed in [11]. Figs. 3 and 4 also show a remarkable change in magnetic flux density calculated for a path in the air gap near the surface of the MSM element. This illustrates the effects of non-homogeneous MSM permeability on the applied magnetic field. The applied field is relatively strong reaching 0.71 T.

A 45° tilt of twin boundaries is an important feature of MSM twin variant geometry [13]. The field lines tend to change their direction inside the MSM element experiencing further bending on twin boundaries. Therefore, the magnetic field vectors in a multi-variant MSM region have both horizontal  $x$ - and vertical  $y$ -spatial components, unlike the air-gap region where magnetic field vectors have a predominant  $x$ -component. Fig. 5 (a) illustrates how initially horizontal magnetic field lines bend due to the internal magnetization of twin variants. Even a very small  $y$ -component of magnetic flux density in the air gap gives rise to a relatively large  $y$ -component of magnetic flux density in a “hard” variant due to large permeability of its “easy” axis. This phenomenon is the most apparent in weak fields. Nevertheless, the overall behavior of the total vector  $\mathbf{B}$  is determined by both  $x$ - and  $y$ -spatial components which depend on magnetic properties of both  $x$ - and  $y$ -axes in a variant. This also emphasizes the importance of analyzing the MSM element as part of the complete magnetic circuit since the geometry of the flux guide affects the magnetic field distribution in the air gap.

**Fig. 5 HERE**

### C. Behavior of the Magnetic Field at a Twin Boundary

The magnetic field lines inside the MSM region change their orientation when crossing twin boundaries, which indicates a significant difference in magnetic field intensity and flux density in “easy” and “hard” variants. The magnetic field continuity equations (6) and (7) can be used for analyzing the behavior of the magnetic field at a twin boundary [16]. Subscripts  $h$  and  $e$  stand for “hard” and “easy” variants, whereas subscripts  $n$  and  $\tau$  stand for normal and tangential components of magnetic field vectors, respectively.

$$B_{hn} = B_{en} \quad (6)$$

$$H_{h\tau} = H_{e\tau} \quad (7)$$

Table 1 summarizes the results obtained for one point on a twin boundary shared by mesh elements that lie in different

variants. The error in continuity equations (6) and (7) in the obtained solution does not exceed  $2 \times 10^{-3}$  % illustrating its accuracy. Normal and tangential components of the magnetic field vectors are calculated using  $x$ - and  $y$ -components applying simple trigonometry to the problem illustrated in Fig. 6. The mutual orientation of field lines is consistent with the magnetic field in Fig. 5. It is remarkable that almost negligible 0.002T  $B_y$  component of the magnetic flux density in the air gap gives rise to considerable longitudinal fields inside twin variants. This makes calculation of the magnetic field in the MSM region using analytical methods very complicated. Therefore, application of FEA is essential for obtaining accurate magnetic field distribution in magnetic circuit of an actuator with a non-homogeneous MSM element due to the geometry of its twin variants and associated magnetic anisotropy.

**TABLE 1 HERE**

**Fig. 6 HERE**

Table 1 illustrates the significant difference between the magnetic fields inside “hard” and “easy” variants. Moreover, relative permeability calculated using total flux density and field intensity lies neither on “hard” nor on “easy” magnetization curves. This can be expected for anisotropic regions since magnetization curves in Fig. 2 guide only  $x$ - and  $y$ -components of vectors related to “easy” and “hard” magnetization axes. It is also important that magnetic field intensity differ between MSM and air gap regions. Table 1 shows that the difference in magnetic field intensity reaches one order of magnitude for the studied magnetic field distribution. This illustrates the significance of demagnetization effects usually neglected in other models. This result can be particularly important for single twin boundary MSM elements that operate in very weak magnetic fields.

### D. Applicability of Simplistic Equivalent Electric Circuit Models

The application of an electric circuit equivalent of the magnetic circuit can be very beneficial for preliminary design owing to the simplicity of the approach [16]. Since only a parallel or series connection of reluctances in a circuit is possible, it is necessary to determine how MSM twin variants are connected magnetically. The parallel connection of elements corresponds to magnetic field lines passing through either “hard” or “easy” variants, whereas magnetic field intensity  $\mathbf{H}$  should be the same for both types of variants. However, the data in Table 1 and magnetic field distribution in Fig. 5 show that these conditions are not satisfied. On the contrary, each field line is passing through both “easy” and “hard” variants suggesting that variants are connected in series. However, field lines change their orientation bending

on twin boundaries due to anisotropy of MSM twin variants. Hence, neither parallel nor series connection of variants can represent the real magnetic field distribution correctly.

It is remarkable that the 45° tilt of twin boundaries is the main reason for the inapplicability of equivalent circuit models to multi-variant MSM regions. The magnetic field distribution in an imaginary MSM element with horizontal twin boundaries in Fig. 7 (a) can be approximated by parallel connection of elements since field lines are passing through either “hard” or “easy” variants. Straightening of field lines implies negligible  $y$ -spatial component of the magnetic flux density in MSM twin variants which satisfies the necessary conditions for a branch of an equivalent circuit. This illustrates the significant effect of the angle between twin boundaries and the surface of the MSM element on the magnetic field distribution.

However, it is still possible to represent a single-variant MSM element by a single reluctance with reasonable accuracy since the magnetic field in Fig. 2 is almost homogeneous. Similarly, a sufficiently strong magnetic field can saturate “easy” variants in a blocked MSM element resulting in field lines aligning with the bias field, as shown in Fig. 7 (b). In this case, straightening of the field lines is a consequence of change in permeability unlike the change in geometry shown in Fig. 7 (a). This is obtained by applying a magnetic field of 1 T which exceeds the saturation flux density of the MSM element. This leads to a decrease in «easy» variants' relative permeability to that of «hard» variants' resulting in a uniform magnetic field distribution.

**Fig. 7 HERE**

### III. VALIDATION OF THE PROPOSED APPROACH

The results of inductance measurement published by Suorsa *et al.* in [17] are used for validating the proposed approach. Those results show that neither parallel nor series connection of twin variants in an equivalent circuit model can predict the behavior of varying MSM permeability correctly. The reason for such a behavior has not been identified. However, this result correlates with the discussion in Section II. In this Section we are modeling the same setup in order to determine whether the reported change in inductance can be explained using the approach proposed in this paper.

An equivalent circuit model of the setup is used in addition to FE models for different strains in a mechanically blocked MSM element. Since the properties of the MSM element in the experiment are measured as of a single object, its real non-homogeneous microstructure is treated as a homogeneous element with equivalent permeability. Therefore, a circuit model can be implemented where the MSM element is represented by a single reluctance replicating the experiment. Due to simplicity of the magnetic circuit in Fig. 8 (a), it is possible to find such a reluctance and corresponding

equivalent MSM permeability that allows obtaining the same solution in both FE and equivalent circuit models. This allows comparison of the experimental data reported in [17] with the modeling results obtained in this study. It should be stressed that whilst the application of the circuit model requires MSM element to be in a single-variant state, its twinned microstructure is modeled explicitly in the FE model using the approach discussed above.

**Fig. 8 HERE**

Equations for a branch of the equivalent magnetic circuit in Fig. 8 (b) can be written as

$$F_\delta = \sum_\delta H_\delta \delta + \sum_{a_m} H_{msm} a_m \quad (8)$$

$$\Phi_\delta = F_\delta / (R_\delta + R_{msm}) \quad (9)$$

$$R_\delta = (\delta + a_m \varepsilon) / \mu_0 A_\delta \quad (10)$$

$$R_{msm} = a_m (1 - \varepsilon) / \mu_0 \mu_m A_m \quad (11)$$

where  $F_\delta$  is mmf drop along the air gap length, A,  $H_\delta$  and  $H_{msm}$  are magnetic field intensities in the air gap and MSM regions respectively, A/m,  $\delta$  is total width of air gaps between the MSM element and the poles, m,  $a_m$  is width of the MSM element, m,  $R_\delta$  is air gap reluctance, 1/H;  $R_{msm}$  is reluctance of the MSM element, 1/H,  $\varepsilon$  is relative strain,  $\mu_0$  is absolute permeability of vacuum, H/m,  $\mu_m$  is equivalent relative permeability of the MSM element,  $A_\delta$  and  $A_{msm}$  are air gap and MSM element cross-sectional areas respectively normal to the magnetic flux, m<sup>2</sup>. By rearranging (8)–(11) with respect to strain dependent MSM permeability, the final equation yields

$$\mu_m = B_\delta a_m (1 - \varepsilon) / [F_\delta \mu_0 - B_\delta (\delta + a_m \varepsilon)] \quad (12)$$

where  $B_\delta$  is average magnetic flux density in the air gap near the surface of the MSM element, T. The air gap width at zero strain is 0.2 mm in the studied magnetic circuit. It should be stressed that this approach requires no assumptions regarding the magnetic connection of twin variants.

In order to replicate the experiment conducted in [17], the input current was kept constant whereas strain of the MSM element was variable.  $B_\delta$  and  $F_\delta$  extracted from the FE solution were used as input data for (12) along with geometric parameters of the air gap and MSM element. Fig. 9 shows how the calculated equivalent relative permeability of MSM element varies with its strain. The changes in MSM permeability predicted by series and parallel connection of twin variants are also plotted for reference. As can be expected after analyzing Table 1, the graph corresponding to equivalent MSM permeability lies between the graphs corresponding to series and parallel connection of elements exhibiting strong non-linear behavior. It should be stressed that this result holds for weak fields where “easy” variants are not saturated. Since “easy” axis permeability decreases in stronger fields, all three graphs will tend to get closer to the horizontal axis in such

cases. Nevertheless, the general trend of the graphs in Fig. 9 is the same even in strong magnetic fields.

### Fig. 9 HERE

Finally, the inductance of the coil calculated using the modeling results is compared with those obtained from measurements in [17]. Equation (13) allows the calculation of coil inductance depending on strain and corresponding equivalent permeability of the MSM element

$$L = L_{\sigma} + N^2 \mu_0 A_m \mu_m / [a_m + \mu_m \delta + (\mu_m - 1) a_m \varepsilon] \quad (13)$$

where  $L_{\sigma}$  is leakage inductance,  $H$ , and  $N$  is the number of coil turns. In order to verify the approach, (13) is solved using the data listed in Table 1 in [17] and relative permeability of MSM element obtained in this study. The results are shown in Fig. 10. The graphs calculated with the assumption of parallel and series connection of MSM twin variants are also plotted for reference. It should be noted that the leakage inductance  $L_{\sigma}$  is used only for calibrating the zero point of these graphs. The behavior of the graph obtained using the proposed modeling approach is very similar to that of the experimental graphs obtained by measurement in Fig. 9 in [17]. This shows that the proposed approach can be used for predicting the reported change in inductance and, hence takes varying MSM permeability into account correctly. Therefore, the proposed approach allows quantitative estimation of MSM permeability changes which is essential for actuator and sensor design. Fig. 10 shows that the total change in inductance exceeds 50%. This illustrates how significant the change in MSM permeability is, since it is the only varying parameter in this particular setup.

## IV. DISCUSSIONS

The application of the proposed approach to modeling the MSM element in actuators reveals several important aspects of magnetic field distribution in the magnetic circuit. First, the magnetic fields in MSM and air gap regions are considerably different because of demagnetization. Moreover, the air gap magnetic field is very non-uniform in the vicinity of non-homogeneous MSM element, as shown in Figs. 3 and 4. This illustrates how the position of a Hall sensor can affect the measurement results, especially when the “easy” fraction is concentrated in a particular area of the MSM element. This is particularly relevant for MSM elements with a single, highly-mobile twin boundary. Nevertheless, this effect still occurs in the vicinity of a multi-variant MSM element with fine twins.

Second, the magnetic field distribution is very non-uniform in non-homogeneous multi-variant MSM elements. In addition, the crystal anisotropy has significant effects on the magnetic field distribution. The magnetic field lines tend to

align with “easy” axes in twin variants due to their large initial permeability. However, this affects the magnetic field distribution in “hard” variants as well as in “easy” variants. This effect cannot be taken into account accurately if MSM twin variants are considered isotropic. Moreover, this questions the applicability of approaches that consider the MSM element as a homogeneous “black box” element in magnetic circuit. The most well-known model used for evaluating magnetic field-induced stress is developed by Likhachev and Ullakko [18]. Several other models have been later developed based on this e.g., in [19], [20]. However, these are essentially 1-D models that neither take into account demagnetization nor non-homogeneity of the MSM element. This leads to an assumption that the magnetic field intensity is uniform throughout both MSM and air gap regions. Results summarized in Table 1 show that such an assumption is not exactly valid. The flux density and magnetic field intensity can vary significantly among twin variants. This also affects the magnetic field distribution in the air gap. Therefore, a model for calculating magnetic field-induced stresses taking into account non-homogeneous nature of the magnetic field distribution as well as magnetic anisotropy of twin variants is needed. Since a longitudinally applied magnetic field produces a compressive stress in the MSM element (as shown in Fig. 1 (b)), the bending of magnetic field lines inside the MSM region implies production of compressive stresses along with tensile stresses acting on a twin boundary [13]. Thus, simplistic models would predict larger output stress and, hence larger output force of an actuator than a model that takes all the above effects into account. Accurate incorporation of magnetic field distribution in the MSM region is essential for optimal design of MSM-based devices. Simplified models can be justified for special cases derived from a more accurate and complete model.

The modelled non-uniform distribution of magnetic field inside a twinned MSM element in a transversely applied external field questions the common assumption that such orientation of the bias field is optimal for actuation. The topic of optimal field orientation goes all the way back to the very beginning of MSM research. For instance, it was proposed that for strongly anisotropic MSM element the optimal orientation of the applied field coincides with the twin boundary [21]. This paper shows that FE modelling can be successfully applied to study the mutual interaction between anisotropic MSM elements and the applied field taking into account all the important features of the twinned MSM microstructure. Therefore, the effects of different orientations of the source field on the magnetic-field induced stress can also be studied given that an expression for stress calculation is available.

Fig. 9 shows a very non-linear behavior of varying equivalent permeability of the MSM element when it is considered as a single element. However, the relative permeability calculations summarized in Table 1 show that it also differs between different variants. Moreover, the anisotropy of crystal poses a challenge for analytical calculation of MSM permeability making FE analysis an important and necessary tool for modeling the MSM element.

The non-linear magnetic behavior of “easy” axis and potential saturation of MSM twin variants also have significant effects on magnetic field distribution in the MSM element and, hence on the magnetic circuit of an actuator as a whole. Magnetic circuit models can be also applied to a very limited number of cases due to the inadequacy of series and parallel connection of reluctances to describe magnetic connections of twin variants in MSM elements with fine twins.

The total reluctance of magnetic circuit of an actuator with a core made of high-permeable magnetic material is mainly determined by the reluctance of its air gap region. In case of MSM actuators, this reluctance is a sum of air-region reluctance and the reluctance of the MSM element. By analyzing (11) together with the behavior of MSM permeability in Fig. 9, it can be concluded that MSM reluctance always decreases with strain. However, the opposite is true for air gap reluctance (10). Therefore, the overall change in the reluctance of magnetic circuit depends on the ratio of these two reluctances. Nevertheless, for MSM actuators with a narrow air gap, the change in MSM reluctance prevails over the change in reluctance of the air regions. Since minimizing the air gap is one of the important objectives in actuator design, this behavior can be assumed to be true in general. However, one should take extra care when very strong magnetic fields (that result in saturation of MSM twin variants) are considered.

Whereas 2D models were used in this study primarily due to the opportunity to plot flux lines, the proposed modeling approach is perfectly applicable to 3D modeling. Since  $b$  axis is essentially another “hard” magnetization axis, it can be treated the same way as  $a$  axis in the model. However, no difference in the behavior of the MSM permeability in 3D can be expected as long as the magnetic field is plane-parallel. Nevertheless, 3D modeling is vital for accurate modeling of the complete magnetic circuit which would allow taking into account effects attributable to 3D flux leakage.

## V. CONCLUSIONS

Magnetic field distribution in non-homogeneous MSM element is studied using a FE modeling approach. Its non-homogeneous microstructure is taken into account along with particular geometry of MSM twin variants and their non-linear anisotropic magnetic properties. The FE analyses show a considerable difference in magnetic field distribution between air gap and MSM regions due to demagnetization effects. A very non-uniform distribution of magnetic field in a multi-variant MSM element is also discussed by analyzing the effects related to twin variant geometry, non-homogeneity and magnetic anisotropy of MSM crystals.

The proposed modeling approach is successfully applied for the calculation of previously reported results obtained by inductance measurement. This validates its applicability to the evaluation of variable permeability MSM elements. The ability to model the MSM element as part of a complete magnetic circuit is also essential for actuator and sensor design. This allows the study of mutual effects of different

elements of magnetic circuit, which is vital for design optimization.

## REFERENCES

- [1] A. A. Likhachev and K. Ullakko, “Magnetic-field-controlled twin boundaries motion and giant magneto-mechanical effects in Ni–Mn–Ga shape memory alloy,” *Phys. Lett. A*, vol. 275, pp. 142–151, Oct. 2000.
- [2] S. J. Murray, M. Marioni, S. M. Allen, and R. C. O’Handley, “6% magnetic-field-induced strain by twin-boundary motion in ferromagnetic NiMnGa,” *Appl. Phys. Lett.*, vol. 77, no. 6, pp. 886–888, 2000.
- [3] A. Sozinov, N. Lanska, A. Soroka, and W. Zou, “12% magnetic field-induced strain in Ni-Mn-Ga-based non-modulated martensite,” *Appl. Phys. Lett.*, vol. 102, no. 2, p. 021902, Jan. 2013.
- [4] O. Heczko and K. Ullakko, “Effect of Temperature on Magnetic Properties of Ni – Mn – Ga Magnetic Shape Memory ( MSM ) Alloys,” *IEEE Trans. Magn.*, vol. 37, no. 4, pp. 2672–2674, 2001.
- [5] I. Aaltio, Y. Ge, H. Pulkkinen, A. Sjöberg, O. Söderberg, X. W. Liu, and S. P. Hannula, “Crack growth of 10M Ni-Mn-Ga material in cyclic mechanical loading,” *Phys. Procedia*, vol. 10, pp. 87–93, Jan. 2010.
- [6] O. Heczko, V. Kopecky, L. Fekete, K. Jurek, J. Kopecek, L. Straka, and H. Seiner, “Magnetic Domains and Twin Microstructure of Single Crystal Ni-Mn-Ga Exhibiting Magnetic Shape Memory Effect,” *IEEE Trans. Magn.*, vol. 51, no. 11, pp. 15–18, 2015.
- [7] S. Barker, E. Rhoads, P. Lindquist, M. Vreugdenhill, and P. Müllner, “Micropump utilizing localized magnetic-field-induced deformation of MSM elements to deliver sub-microliter volumes of drugs to the rat brain,” *Proc. Actuator*, pp. 96–97, 2014.
- [8] J. Ziske, F. Ehle, H. Neubert, A. Price, and J. Lienig, “A simple phenomenological model for Magnetic Shape Memory Actuators,” *IEEE Trans. Magn.*, vol. 51, no. 1, p. 4002608, 2015.
- [9] F. Auricchio, A.-L. Bessoud, A. Reali, and U. Stefanelli, “A phenomenological model for the magneto-mechanical response of single-crystal magnetic shape memory alloys,” *Eur. J. Mech. A/Solids*, vol. 52, pp. 1–11, 2015.
- [10] K. Haldar, G. Chatzigeorgiou, and D. C. Lagoudas, “Single crystal anisotropy and coupled stability analysis for variant reorientation in Magnetic Shape Memory Alloys,” *Eur. J. Mech. - A/Solids*, vol. 54, pp. 53–73, 2015.
- [11] O. Heczko, D. Vokoun, V. Kopecky, and M. Beleggia, “Effect of magnetostatic interactions on twin boundary motion in NiMnGa Magnetic Shape Memory Alloy,” *IEEE Magn. Lett.*, vol. 6, pp. 1–4, 2015.
- [12] O. Heczko, L. Straka, and S.-P. Hannula, “Stress dependence of magnetic shape memory effect and its model,” *Mater. Sci. Eng. A*, vol. 438–440, pp. 1003–1006, Nov. 2006.
- [13] T. Schiepp, M. Maier, E. Pagounis, A. Schlüter, and M. Laufenberg, “FEM-Simulation of Magnetic Shape Memory Actuators,” *IEEE Trans. Magn.*, vol. 50, no. 2, p. 7024504, 2014.
- [14] E. Pagounis, M. Maier, and M. Laufenberg, “Properties of large Ni-Mn-Ga single crystals with a predominant 5M-martensitic structure,” *3rd Int. Conf. Ferromagn. Shape Mem. Alloy.*, pp. 207–208, 2011.
- [15] L. Straka, H. Hänninen, A. Soroka, and A. Sozinov, “Ni-Mn-Ga single crystals with very low twinning stress,” *J. Phys. Conf. Ser.*, vol. 303, p. 012079, Jul. 2011.
- [16] M. Nayfeh and M. Brussel, *Electricity and Magnetism*. New York: John Wiley & Sons, 1985.
- [17] I. Suorsa, E. Pagounis, and K. Ullakko, “Position dependent inductance based on magnetic shape memory materials,” *Sensors Actuators, A Phys.*, vol. 121, pp. 136–141, May 2005.
- [18] A. A. Likhachev and K. Ullakko, “Quantitative Model of Large Magnetostrain Effect in Ferromagnetic Shape Memory Alloys,” *EPJ Direct*, vol. B2, pp. 1–9, 1999.
- [19] L. Straka and O. Heczko, “Superelastic Response of Ni – Mn – Ga Martensite in Magnetic Fields and a Simple Model,” *IEEE Trans. Magn.*, vol. 39, no. 5, pp. 3402–3404, 2003.
- [20] A. A. Likhachev, A. Sozinov, and K. Ullakko, “Different modeling concepts of magnetic shape memory and their comparison with some experimental results obtained in Ni–Mn–Ga,” *Mater. Sci. Eng. A*, vol. 378, no. 1–2, pp. 513–518, Jul. 2004.

[21] R. C. O'Handley, "Model for strain and magnetization in magnetic shape-memory alloys," *Jour. App. Phys.*, vol. 83, no. 6, p. 3263, 1998.

**N. Gabdullin (S'13)** received his M.Sc. degree (first degree) with Distinction in electrical engineering, electromechanics and electrotechnologies in 2012 (2006-2012) from National Research University "Moscow Power Engineering Institute", Moscow, Russia.

He is currently a PhD candidate in Electrical and Electronic Engineering in the School of Mathematics, Computer Science and Engineering at City, University of London, London, U.K. His research interests include electromagnetic field analyses using numerical techniques, such as FEM and its application to the study of magneto-mechanical behavior of MSM alloys, MSM actuator design and optimization, and thermal characterization of electromagnetic devices.

**S. H. Khan (M'90)** received the M.Sc. (Hons.) degree in electromechanical engineering and the Ph.D. degree in electrical engineering from Peter the Great St. Petersburg Polytechnic University (SPPU), Saint Petersburg, Russia, in 1983 and 1988, respectively.

He started his Ph.D. research with Peter the Great St Petersburg Polytechnic University in 1984. He defended the Ph.D. thesis in 1987. He has been with the School of Mathematics, Computer Science and Engineering, City, University of London, London, U.K., since 1989, where he is a Professor of Instrumentation and Sensors. He is an active member with the Photonics and Instrumentation Research Centre, School of Mathematics, Computer Science and Engineering, City, University of London. He has published many papers in journals, conferences, and in books. His current research interests include mathematical modeling and CAD of sensors, instruments and devices, computational electromagnetics, finite element modeling and numerical methods, and forward and inverse problems in tomographic imaging.

Professor Khan is a Fellow of The Institution of Engineering and Technology (IET) and the Institute of Measurement and Control (InstMC), and a member of the IEEE Magnetics Society. He is an Honorary Professor of SPPU. He was a Vice President of InstMC from 2008 to 2011. He is also a Founder Member of the International Compumag Society and a member of the Journal Editorial Committee of *Measurement and Control*. He is an Associate Editor of the *Measurement* journal, and the *International Journal on Measurement Technologies and Instrumentation Engineering*.

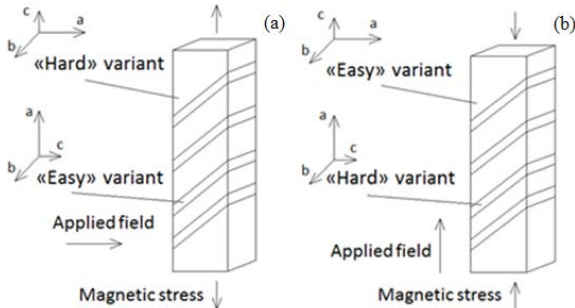


Fig. 1. Orientation of crystallographic axes in twin variants of MSM element: (a) transversely and (b) longitudinally applied magnetic field.

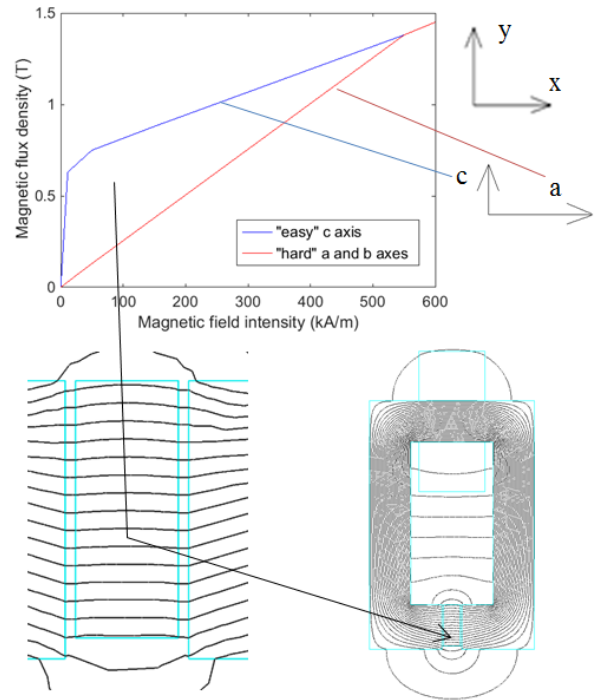


Fig. 2. B-H curves for "hard" and "easy" magnetization axes of anisotropic single-variant MSM element in 2D model of magnetic circuit of an actuator.

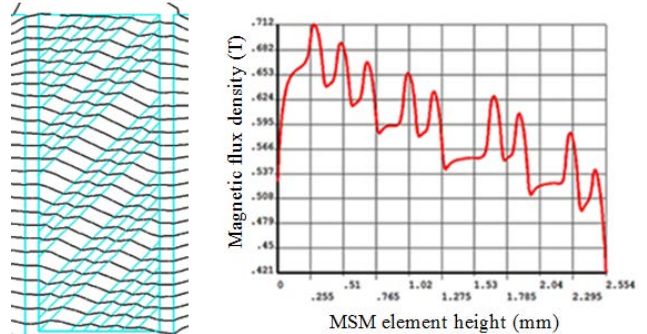


Fig. 3. Magnetic field lines in the MSM element with fine twins and x-component of magnetic flux density in the air gap near the left surface of the MSM element. "Easy" variants constitute 36% of the volume.

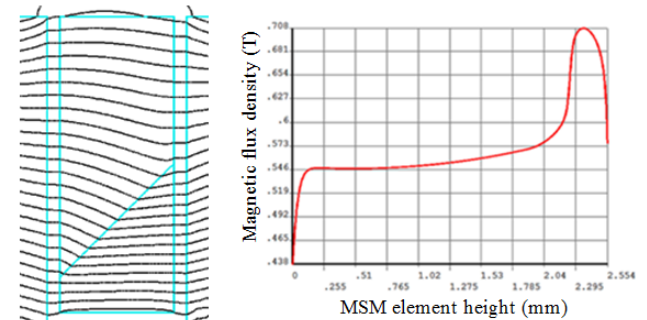


Fig. 4. Magnetic field lines in the MSM element with a single twin boundary and x-component of magnetic flux density in the air gap near the left surface of the MSM element. "Easy" variants constitute 36% of the volume.

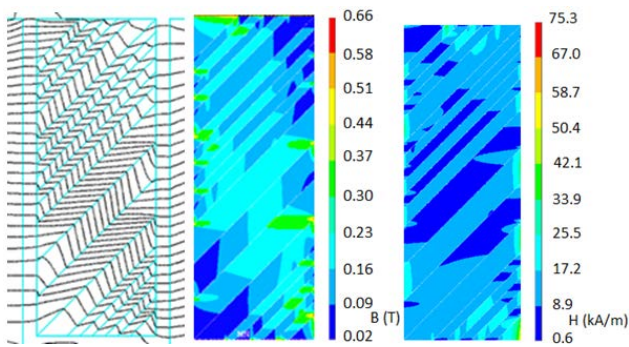


Fig. 5. Magnetic field lines in MSM element with fine twins in a weak bias magnetic field and corresponding flux density and field intensity plots.

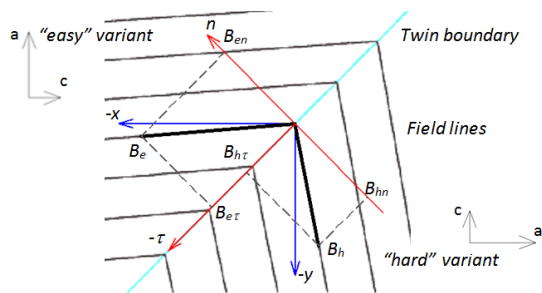


Fig. 6. Projections of magnetic flux density vectors in "easy" and "hard" variants on different axes associated with the twin boundary.

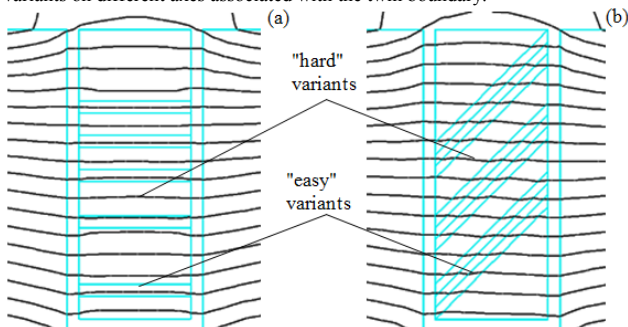


Fig. 7. Magnetic field lines in MSM elements with (a) horizontal twin boundaries in a weak magnetic field and (b) twin boundaries of actual geometry in a magnetic field strong enough for saturating "easy" variants.

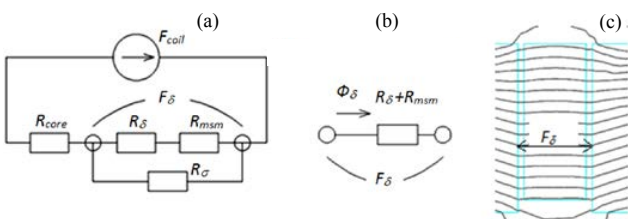


Fig. 8. An equivalent electric circuit of the magnetic circuit used in the experimental setup in [17]. (a) Representation of the complete circuit, (b) its air gap region with the MSM specimen and (c) corresponding air gap region in a FE model.

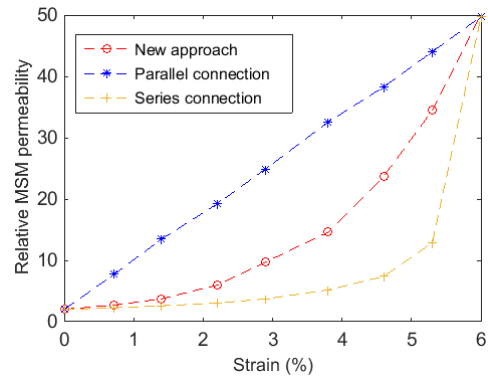


Fig. 9. Change in equivalent relative permeability of the MSM element due to the change in its strain.

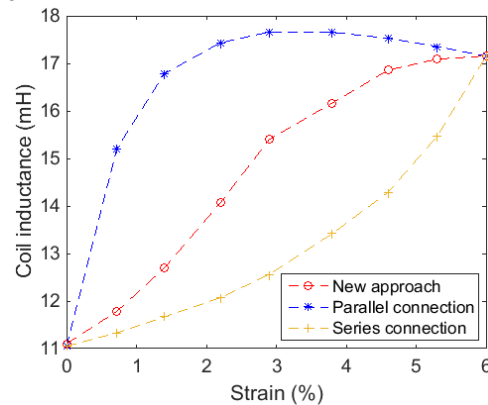


Fig. 10. Change in the inductance of measurement coil due to the change in strain of the MSM element.

TABLE I  
Components of  $\mathbf{B}$  and  $\mathbf{H}$  Calculated for a Single Point at a Twin Boundary Shared by "Easy" and "Hard" Variants

	"hard"	"easy"	air gap <sup>a</sup>
$B$ , T	0.162	0.212	0.128
$B_x$ , T	0.036	0.211	0.128
$B_y$ , T	-0.158	0.019	0.002
$H$ , kA/m	13.59	8.17	101.98
$H_x$ , kA/m	13.35	3.37	101.96
$H_y$ , kA/m	-2.53	7.45	1.78
$\mu_r$	9.5	20.6	1
$\mu_x$	2	50	1
$\mu_y$	50	2	1
$B_n$ , T	0.13578	0.13578	-
$H_\tau$ , kA/m	7.6507	7.6507	-

<sup>a</sup>Air gap region results are provided for reference